A Missing Solution to the Transport Equation and Its Effect on Estimation of Cloud Absorptive Properties

Y. KNYAZIKHIN

Department of Geography, Boston University, Boston, Massachusetts

A. MARSHAK

Joint Center for Earth System Technology, University of Maryland, Baltimore County, Baltimore, and Climate and Radiation Branch, NASA Goddard Space Flight Center, Greenbelt, Maryland

W. J. WISCOMBE

Climate and Radiation Branch, NASA Goddard Space Flight Center, Greenbelt, Maryland

J. V. MARTONCHIK

Jet Propulsion Laboratory, California Insitute of Technology, Pasadena, California

R. B. MYNENI

Department of Geography, Boston University, Boston, Massachusetts

ABSTRACT

Most of the existing cloud radiation models treat liquid water drops of a variety of sizes as an ensemble of particles. The ensemble approach assumes that all drop sizes are well represented in an elementary volume, and its scattering and absorbing properties can be accurately specified through the use of the drop size probability density distribution function. The concentration of large drops, however, can be so low that a chance to capture them in the elementary volume is rare. Thus the drop ensemble assumption is not always true, though classical radiative transfer theory uses this assumption to simplify the radiative transfer process, as if scattering takes place from an ''average drop'' rather than from a particular drop. The theoretical analysis presented in this paper demonstrates that if a cumulative distribution function is used to describe drop size variability with jumps accounting for the probability of finding large drops in the elementary volume, one obtains an extra term, the Green's function, in the solution of the radiative transfer equation. The analysis of data on cloud drop size distribution acquired during the First International Satellite Cloud Climatology Project (ISCCP) Research Experiment (FIRE) field campaign clearly shows jumps in the cumulative drop size distribution; the magnitudes of the jumps are related to the frequencies of large drop occurrence. This discontinuity is primarily responsible for the additional terms that must be added to the solution to properly account for the photon interaction with the large drops. The enhancement of cloud absorption due to accounting for the ''missing solution'' exhibits a jump-like response to continuous variation in the concentration of large drops and may exceed the enhancement predicted by the ensemble-based models. The results presented here indicate that the missing term might be plausible to explain the enhanced value of the ratio of the shortwave cloud forcing at the surface to the forcing at top of the atmosphere.

1. Introduction

Recent studies indicate that the atmosphere absorbs more solar radiation than any current model can predict

Corresponding author address: Y. Knyazikhin, Dept. of Geography, Boston University, 675 Commonwealth Ave., Boston, MA 02215.
E-mail: jknjazi@crsa.bu.edu

(Cess et al. 1995, 1999; Ramanathan et al. 1995; Pilewski and Valero 1995; Valero et al. 2000). If true (Stephens 1996; Asano et al. 2000), this excess absorption can be due to the cloudy atmosphere (Zender et al. 1997; Collins 1998) or water vapor absorption in clear sky (Arking 1996, 1999). If we assume that a cloudy atmosphere absorbs more than one-dimensional radiative transfer theory predicts, the most natural explanation would be in the radiative effects of the three-di-

mensional cloud structure or broken cloudiness. In other words, cloud inhomogeneity would give longer photon paths. However, extensive numerical calculations based on different three-dimensional cloud structures (stochastic models or satellite-retrieved scenes) failed to find photon paths long enough to explain the excess absorption (Barker et al. 1998; Marshak et al. 1998; O'Hirok et al. 2000). Thus, neither one-dimensional nor three-dimensional theories can explain the enhanced cloud absorption.

In spite of the diversity of published approaches and techniques used to analyze the absorption anomaly (Stephens and Tsay 1990), they all are based on the assumption that drops behave as an ensemble of particles (Liou 1992, p. 255). The notion of "ensemble" is based on the assumption that an elementary volume has either all drop sizes or no drops at all. A realistic cloud contains a huge number of small drops and a tiny number of large ones; hence, the latter cannot be present in every elementary volume. To stay in the framework of the ensemble approach, large drops are artificially fractionated (included in concentrations less than 1 per elementary volume) even though this is obviously a poor approximation since drops are discrete. This step is followed by the derivation of the drop size density distribution function. Stated differently, one first averages the drop concentration over space, evaluates the extinction coefficient and scattering phase function and then solves the radiative transfer equation with average characteristics. An alternative technique is first to solve the radiative transfer equation for each realization of drop sizes and then to average solutions over all possible realizations. The latter does not rely on the ensemble concept. The cumulative drop size distribution function is necessary to describe drop variability in this case. With a simple example, we show that radiances obtained by these two techniques differ by the Green's function (section 2). We expressed the radiative transfer equation in terms of the cumulative distribution function. If this function is smooth enough, its solution coincides with one obtainable under the ensemble assumption. However, the presence of jumps in it leads to the appearance of an additional term in the solution, which may enhance the cloud absorptivity. This finding suggests that the ensemble-based models may underestimate the cloud absorption if the condition of their applicability is not met.

We analyzed data on cloud drop size distribution acquired during the First International Satellite Cloud Climatology Project (ISCCP) Research Experiment (FIRE) field campaign (section 3 and appendix B). It is shown that the cumulative drop size distribution deduced from measurements is not an absolutely continuous function and we derive parameters that quantify its discontinuity. This leads to an additional component in the solution of the radiative transfer equation, which is required to properly describe the radiation regime in clouds.

Based on the results of section 2 and appendix C, a theoretical analysis of the enhanced value of the ratio of the shortwave cloud forcing at the surface, to the forcing at top of the atmosphere, is presented in section 4. The solution to the radiative transfer equation, which does not rely on the ensemble concept, is treated as the true radiation field in a cloudy atmosphere and is the one provided by measurements. The ensemble-based solution is taken as the model prediction. The ratio depends on the total number of large drops excluded from the ensemble. It is shown that even a very low concentration of such drops can cause an enhanced value of the ratio as reported in the literature (Cess et al. 1995; Ramanathan et al. 1995; Pilewski and Valero 1995; Ramanathan and Vogelmann 1997). The violation of the ensemble assumption, therefore, may lead to the discrepancy between ensemble-based estimates and measurements.

2. Attenuation of radiation by clouds: Theory

The scattering and absorption properties of clouds are determined by scattering and absorption properties of individual cloud drops which, in turn, are functions of the drop size. The drop is referred to as a single homogenous sphere of the radius r. The drop size distribution is the most important variable determining the photon-cloud interaction. We analyze a widely used assumption regarding the drop size distribution, and, with a simple example, demonstrate the effect of its violation on the estimation of cloud radiation regime.

Consider a parallelepiped with the base dS perpendicular to a direction Ω and the height ξ (Fig. 1). A cumulative drop size distribution function $N(r, \xi)$ is defined as the ratio of the total number of drops in the parallelepiped with radii in the interval $[0, r)$ to the base dS. An elementary volume $dV = d\xi dS$ contains $N(r, \xi + d\xi)dS - N(r, \xi)dS$ of such drops. In terms of these notations, the optical distance $d\tau(\xi)$ of an elementary interval $[\xi, \xi + d\xi)$ along the direction Ω takes the form

$$
\begin{aligned}
d\tau(\xi) &= \tau(\xi + d\xi) - \tau(\xi) \\
&= \int_0^\infty \sigma_{\text{ext}}(r)\, d_r[N(r, \xi + d\xi) - N(r, \xi)]. \quad (1)
\end{aligned}
$$

Here, σ_{ext} is the particle extinction cross section, and $d_r N(r, \xi) = N(r + dr, \xi) - N(r, \xi)$. The removal of energy along the direction of photon travel is (Beer's law)

$$
dI + I(\xi)\, d\tau(\xi) = 0, \quad (2)
$$

where $I(\xi)$ is the radiance at the point ξ.

Most of the existing cloud radiation models treat drops with a variety of sizes as an ensemble of particles. These models characterize variation in drop radii by a drop size density distribution function $c(r)$ defined as the ratio of the total number $d[N(r, \xi + d\xi) - N(r, \xi)]dS$ of drops in the volume $dV = d\xi dS$ whose radii
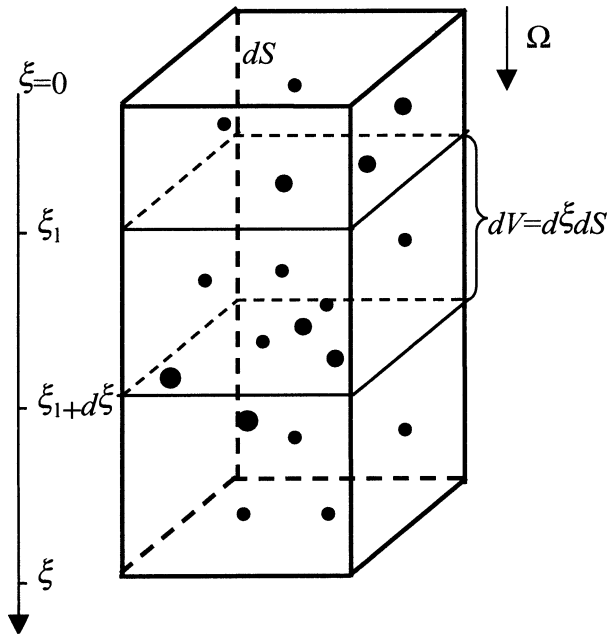
FIG. 1. Parallelepiped with the base dS perpendicular to the direction Ω and the height ξ. A cumulative drop size distribution function $N(r, \xi)$ is defined as the total number of drops in the parallelepiped with radii in the interval $[0, r)$ normalized by dS. The number of drops in an elementary volume $dV = d\xi dS$ is $dNdS = N(r, \xi_1 + d\xi)dS - N(r, \xi_1)dS$.
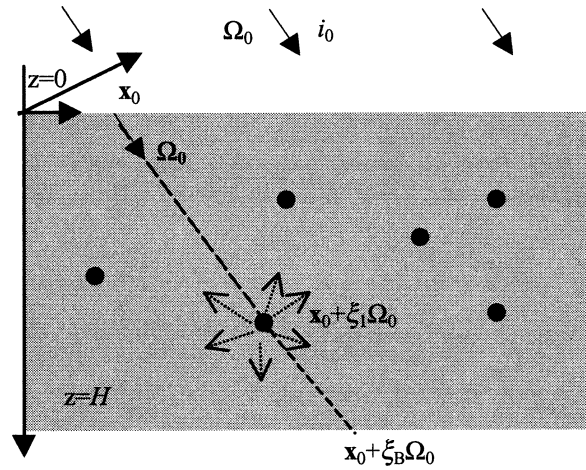

FIG. 2. Schematic representation of photon interactions with the ensemble of particles and individual drops. Elementary volumes that contain all drop sizes with radii from the interval $[r_0, r_E)$ are depicted as a gray area. Drops that can appear in the elementary volume with a low probability are shown as black dots. The direction of an incident beam of intensity i_0 is denoted by Ω_0. Photons entering the cloud through the point $\mathbf{x}_0$ on the upper boundary $z = 0$ and attenuated by the ensemble of particles, experience the first interaction with an individual drop at the point $\mathbf{x}_0 + \xi_1 \Omega_0$. Attenuation of the radiance $I(\xi)$ along the ray $\mathbf{x}_0 + \xi \Omega_0$ is given by equation (7). Its solution is discussed in appendix A. The distance between the point $\mathbf{x}_0$ and the lower boundary along the direction Ω_0 is denoted by ξ_B.

fall in the interval $[r, r + dr)$ to the volume dV and the length dr; that is, (Liou 1992, p. 186)

$$c(r) = \frac{dS d_r [N(r, \xi + d\xi) - N(r, \xi)]}{dS dr d\xi}$$

$$= \frac{d^2 N(r, \xi)}{dr d\xi}. \qquad (3)$$

For simplicity's sake, c is assumed to be independent of ξ. Substituting (3) into (1) results in $d\tau = \sigma_E d\xi$. Here, σ_E is an extinction coefficient for the ensemble of drops. This coefficient is the cross section calculated for a single sphere, averaged over all possible drop radii (Liou 1992, p. 264):

$$\sigma_E = \frac{d\tau}{d\xi} = \int_0^\infty \sigma_{ext}(r) c(r) \, dr. \qquad (4)$$

Here and throughout the text, all variables subscripted by "E" will refer to the ensemble. Equation (2), describing the attenuation of the radiance $I_E(\xi)$ due to photon interactions with the ensemble of particles, rearranges to the form

$$dI_E + \sigma_E I_E(\xi) d\xi = 0. \qquad (5)$$

We assume that the intensity scattered by an elementary volume is the sum of intensities scattered by individual drops (van de Hulst 1981, p. 5; Bohren and Huffman 1983, p. 9). In other words, the elementary volume dV is defined here as a volume inside which

photons can undergo not more than one interaction with drops. The ensemble approach assumes that all drop sizes are well represented in the elementary volume. This yields that scattering and absorbing properties of the elementary volume are proportional to $dV = d\xi dS$ (Zege et al. 1991, p. 16). These assumptions are central to the derivation of Eq. (5). In realistic clouds, the concentration of large drops can be so low that a chance to capture them in the elementary volume is rare. In the framework of the ensemble approach, the elementary volume is defined to contain mainly small droplets. Thus the drop ensemble assumption, which is consistent with the definition of the elementary volume, is not always true. The following example demonstrates the effect of its violation on the estimation of cloud radiation regime.

Consider photon interactions with purely absorbing drops whose radii vary in the interval $r_0 \le r < r_E$. We treat them as the ensemble. Let $C(r, \xi)$ and $c(r)$ be the cumulative drop size distribution function and its density, respectively. It should be emphasized that the ensemble excludes drops of radius r_E in our example, which appear at a finite number of spatial points as shown in Fig. 2. The straight line along the direction Ω_0 of photon travel consists of a "continuous" number of elementary volumes lacking drops of size r_E and one elementary volume that includes such a drop. A cumulative drop size distribution function describing both the ensemble and the single drop along the line (Fig. 2) is given by

$$N(r, \xi) = C(r, \xi) + \mathcal{H}(\xi - \xi_1)\mathcal{H}(r - r_E). \qquad (6)$$

Here, $\mathcal{H}$ is the Heaviside function accounting for the fact that large drops occur at specific locations along the photon path, with specific radii; ξ_1 is the location of the drop r_E on the line $\mathbf{x}_0 + \xi\mathbf{\Omega}_0$. Substituting (6) into (1), and (1) into (2), one obtains an equation that describes the attenuation of the radiance $I(\xi)$ due to photon interactions both with the ensemble and the single drop (see appendix A):

$$dI(\xi) + I(\xi)\sigma_E d\xi + I(\xi)\sigma_{\text{ext}}(r_E)d\mathcal{H}(\xi - \xi_1) = 0. \quad (7)$$

Here, σ_E is the extinction coefficient defined by (4), and σ_{ext} is the particle extinction cross section. The exact solution of this equation is derived in appendix A.

How does the ensemble approach approximate a true solution to Eq. (7)? One first averages the drop concentration over space and evaluates an extinction coefficient $\sigma_E + \Delta\sigma$ using (4). As a result, drops of the radius r_E are included in much smaller fractional concentrations in every elementary volume. Then, one solves the radiative transfer equation (5) with the average extinction coefficient $\sigma_E + \Delta\sigma$. The ensemble based estimate $I_{E+\Delta\sigma}(\xi)$ of the radiation field can be written as

$$I_{E+\Delta\sigma}(\xi) = I_E(\xi) \exp(-\Delta\sigma\xi). \quad (8)$$

Here, $I_E(\xi) = i_0 \exp(-\sigma_E\xi)$ is the solution to (5), and i_0 is the intensity of incident radiation. Because of the sparsity of large drops, $\Delta\sigma$ is relatively small; that is, $\Delta\sigma \ll \sigma_E$. Therefore, solutions $I_E(\xi)$ and $I_{E+\Delta\sigma}(\xi)$ of Eq. (5) corresponding to σ_E and $\sigma_E + \Delta\sigma$ are not significantly distinct.

Let $\Delta(\xi) = I_E(\xi) - I(\xi)$, where $I(\xi)$ is the solution to Eq. (7). Subtracting Eq. (7) from Eq. (5) and taking into account that $dH(\xi - \xi_1)/d\xi = \delta(\xi - \xi_1)$, where δ is the Dirac delta function (appendix A), one obtains

$$\frac{d\Delta}{d\xi} + \sigma_E\Delta(\xi) = I(\xi_1)\sigma_{\text{ext}}(r_E)\delta(\xi - \xi_1).$$

The solution of this equation normalized by $I(\xi_1)\sigma_{\text{ext}}(r_E)$ is the Green's function $G(\xi_1, \xi) = \exp[-\sigma_E(\xi - \xi_1)]\mathcal{H}(\xi - \xi_1)$ for equation (5). Therefore,

$$I(\xi) = I_E(\xi) - I(\xi_1)\sigma_{\text{ext}}(r_E)G(\xi_1, \xi). \quad (9)$$

The true solution (9) includes two types of curves shown in Fig. 3. The first one corresponds to the case when no large drops appear along the photon path. Attenuation of radiance is due to photon interaction with the drop ensemble. This solution is labeled as "Case 1" in Fig. 3. The appearance of a large drop at $\xi = \xi_1$ in the direction of photon travel causes a jump in the true solution $I(\xi)$ at this point (curve "Case 2" in Fig. 3). This has a simple interpretation. Photons entering the medium through the point $\xi = 0$, and attenuated by the ensemble of particles, experience the first interaction with the drop of radius r_E at the point ξ_1 (Fig. 2). The intensity of energy that this drop gains is determined by $I_E(\xi_1)$. The jump in $I(\xi)$ at ξ_1 is the energy that the individual drop removes. The intensity of photons that
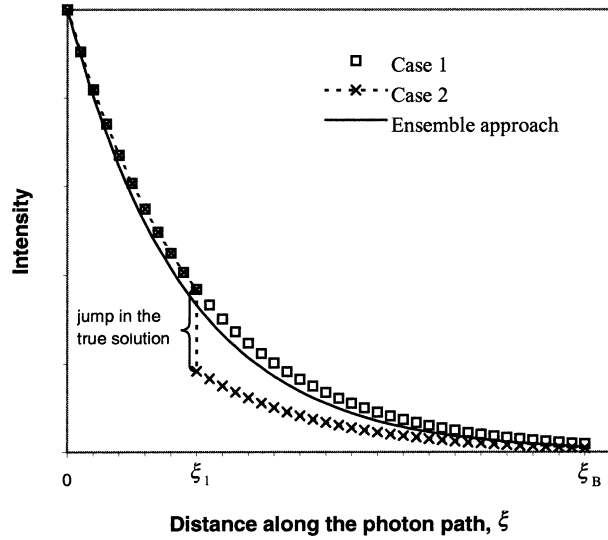

FIG. 3. Attenuation of the radiance along the photon path by the medium shown in Fig. 2. Case 1 has no large drops along the photon path. Case 2 has a large drop at $\xi = \xi_1$ in the direction of photon travel. The curve "ensemble approach" shows the ensemble-based estimate of the true solution.

interacts with the ensemble again is $I(\xi) = I_E(\xi) - I_E(\xi_1)\sigma_{\text{ext}}(r_E)G(\xi_1, \xi)$, $\xi > \xi_1$. The solid line in Fig. 3 schematically shows the ensemble-based estimate $I_{E+\Delta\sigma}(\xi)$ of the true solution.

In our example, the true solution exhibits a piecewise continuous behavior. This means that two different "mechanisms" are involved in the accumulation of energy absorbed by drops. The first one is the integration of radiance over the photon path: the longer the photon path is, the higher the amount of energy that drops absorb. The second one sums jumps in the true solution, each corresponding to a photon path of length zero. This enhances the absorption with the photon path unchanged. The ensemble assumption excludes the latter case and thus may cause a high uncertainty in the estimation of cloud absorptive properties. In other words, the ensemble approach uses a factor $\exp(-\Delta\sigma\xi)$ to force Beer's law to account for the presence of large drops as in Eq. (8) while the correct treatment of large drops yields an addition of an extra term as in Eq. (9). This can lead to the discrepancy between ensemble-based models and measurements that will be theoretically analyzed in section 4.

The mean radiance taken as the average over all possible realizations of drop sizes is a weighted sum of two terms. The first term coincides with $I_E(\xi)$ and accounts for photon–ensemble interaction. The second term is piecewise continuous with jumps accounting for photon interactions with drops excluded from the ensemble. Specification of weights and the radius r_E of the largest drop in the ensemble is discussed in next section. An accurate derivation of this representation in the general case of three-dimensional absorbing and scattering me-

dia is presented in appendix C. The effect of the jumps in the true solution on the estimation of the ratio between the shortwave cloud forcing at the surface and top of the atmosphere will be analyzed in section 4.

3. Drop size distribution: Data analysis

The presence of jumps in the cumulative size distribution is primarily responsible for additional terms in the true solution. These terms account for photon interactions with individual drops and enhance cloud absorptivity with the photon path unchanged. This hypothesis can be confirmed if the cumulative drop size distribution function derived from field measurements does exhibit a jump-like behavior. Aircraft data on liquid water drop sizes is analyzed in this section to see if the cumulative drop size distribution function does exhibit a jump-like behavior.

a. Data used

Two 10-min samples of the cloud drop size distribution measured by the Forward Scattering Spectrometer Probe (FSSP) during the FIRE field program (Albrecht et al. 1988) are used in our analysis. The measurements were taken from 8:44 to 8:54 and 9:31 to 9:41 Pacific daylight time (PDT) on 10 July 1987 over the Pacific Ocean off San Diego. Each flight leg is about 50 km long at an altitude of 725 m in the middle of a 440-m-thick marine stratocumulus cloud layer. The aircraft speed was 80 m s^{-1}, and drops were accumulated over a 1-s time period. The first 10-min sample (from 8:44 to 8:54 PDT) was collected while the aircraft was flying across a ship track [see Fig. 1 in King et al. (1993) for the Geostationary Operational Environmental Satellite (GOES) image of the FIRE marine stratocumulus region with the flight and ship tracks]. The second 10-min sample (from 9:31 to 9:41 PDT) corresponds to the flight along the ship track [see Fig. 5 in King et al. (1990) for the flight track]. The ship track substantially increases cloud drop concentration. In Fig. 4a, the drop concentration increases from 40–50 drops for clean air to 150–200 drops per cubic centimeter for the air mass contaminated by a ship track (see the time intervals between 200 to 250 s and after 650 s). The ship track features enhance the concentration of small drops, reduce the concentration of very large drizzle-like ($r \approx$ 100 μm) drops and narrow the cloud drop size distribution (King et al. 1993). The measured drops are categorized into one of 15 bins with respect to their radii. The bin width is $\Delta r = 2$ μm; radii of the smallest and largest registered drop were $r_0 = 1.4$ μm and $r_{max} = 31.4$ μm, respectively. Thus, each registered drop with radius r belongs to one of $N_{bins} = 15$ intervals $r_{i-1} \le r < r_i$, where $r_i = r_0 + i\Delta r$, $i = 1, 2, \ldots, N_{bins}$; $r_0 = 1.4$ μm, $r_{max} = r_{15} = 31.4$ μm. Figure 4b shows the frequency of occurrence of different values of the number concentration. The measured drop size distributions $c_{obs,k}(r)$, for which the number concentration fell between 166 and 173 were cho-
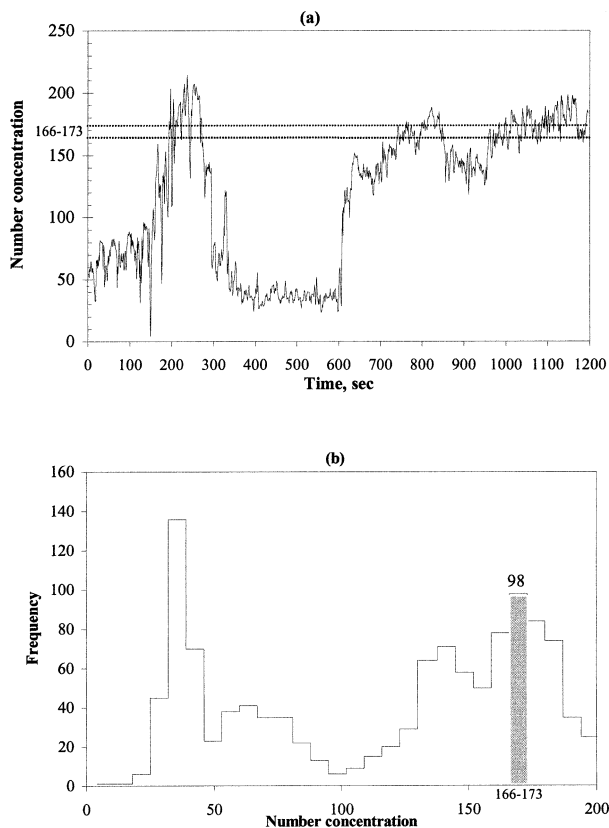
FIG. 4. Drop concentration for the two flight legs between 8:44 and 8:54 and 9:31 and 9:41 PDT on 10 July 1987. Each flight leg is about 50 km long at an altitude of 725 m in the middle of a 440-m-thick marine stratocumulus cloud layer. The first leg is across a ship track, while the second one is along it (King et al. 1990, 1993). (a) Number concentration as a function of time. The time intervals before and after 600 s correspond to the first and second flight legs, respectively. (b) Frequency of the number concentration shown in (a). Drop size distributions for the 98 cases where the number concentration fell in the interval between 166 and 173 were chosen for our analysis.

sen for our analysis. There were $N_{rec} = 98$ drop distributions satisfying this condition. The mean number concentration was 169 drops per cubic centimeter.

b. Results

With the FSSP sample area of $dS = 0.004$ cm^2 (Liu and Hallett 1998) and the distance $d\xi = \xi_k - \xi_{k-1} = 80$ m between two consecutive readings, the kth measurement provides the distribution function $N_k(r) = N(r, \xi_k) - N(r, \xi_{k-1})$ of drop sizes in a volume $dV = dS \times [\xi_{k-1}, \xi_k]$ of 32 cm^3. The interval $[\xi_{k-1}, \xi_k)$ is taken as an elementary interval in our analysis. Our goal is to derive the cumulative drop size distribution function $N(r) = \langle N_k(r) \rangle$, where the angle brackets denote the mean over $N_{rec} = 98$ realizations of the elementary volume. A probabilistic formalism for deriving $N(r)$ is given in appendix B.

Note that the size of FSSP sampling volume does not

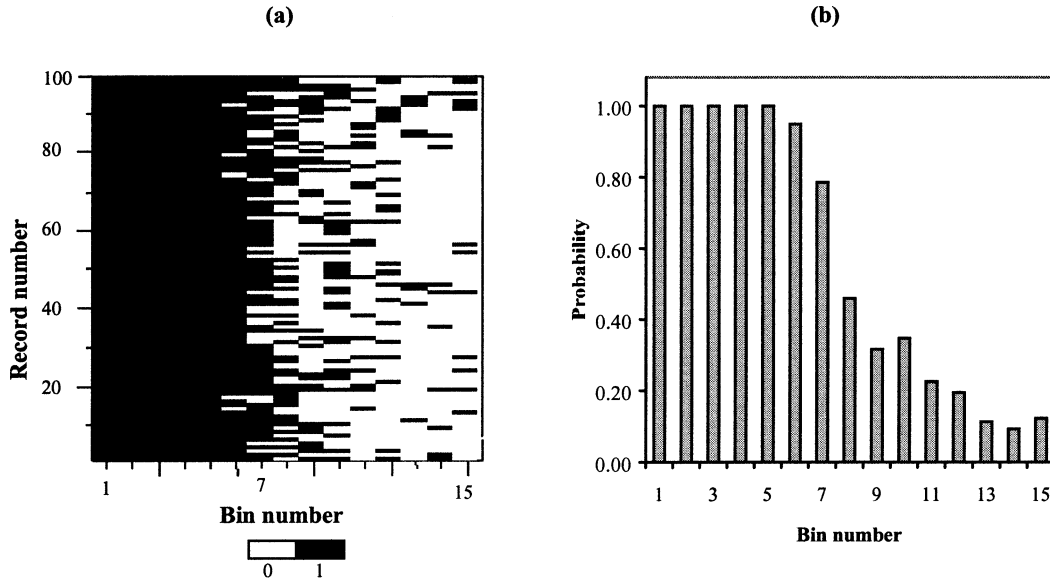**(a)**   **(b)**

FIG. 5. (a) Binary representation of measured drop size distributions. Each row corresponds to one record of the drop distribution whose value at the ith bin of width 2 μm is set to 1 if there is a drop in it, and 0 otherwise. (b) The probability that the FSSP bin contains a drop as a function of the bin number. The ratio between the number of nonempty bins to the total number of records was assigned to the bin number.

necessary coincide with the size of an elementary volume. However, the cumulative distribution function is not tied to its size and thus its specification is not critical to the analysis presented in this section. It also so happens that the 1-s FSSP sampling volume is a tube, and a tube is more like what a photon sees as it travels (Fig. 2). Therefore, the statistics generated by the FSSP can provide enough information to see if the cumulative distribution function exhibits a jump-like behavior along the photon travel as it suggested by Eq. (6).

We start by tackling the following question. How many drops with *different* radii do reside in the 32-cm³
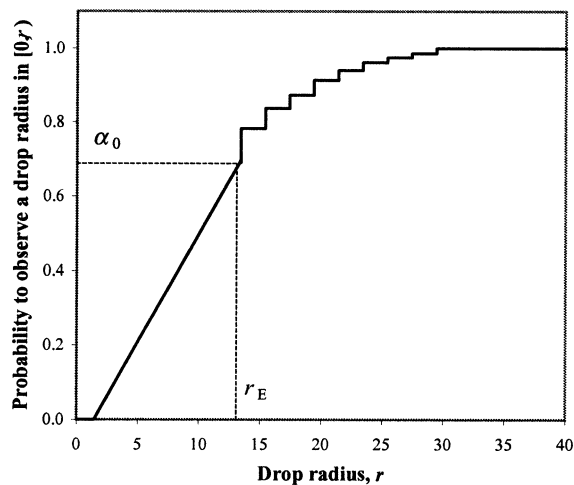

FIG. 6. Fraction $F(r)$ of all registered drop radii present in the interval $[0, r)$. This curve has linear and nonlinear parts. The latter part exhibits a jump-like behavior.

volume? In other words, we want to know how drop sizes, *not drops themselves,* are represented in the elementary volume. Therefore, we focus on examining a binary representation of measured size distributions (Fig. 5a), which *only* provides information on whether a bin is empty or not. It should be emphasized that this information is lost in the framework of the ensemble approach.

Figure 5a demonstrates the appearance of the drop radius in a 2-μm interval while Fig. 5b shows its probability. Clearly, the probability of finding a drop in the 32-cm³ volume falls distinctly below unity starting with bin 7. This figure also suggests that the ensemble assumption is accurate enough for drops below bin 7, but not above. For bins below 7, the total number of drop *radii* that fell in a given interval is proportional to the length of the interval. For example, if an interval, consisting of two consecutive bins (each of width 2 μm) is increased/decreased twice, the number of drop radii in this interval is also increased/decreased twice (Fig. 5a). The ensemble approach assumes this proportionality to hold true independently of the bin width. The proportionality, however, breaks down for drops above bin 7. For example, the interval length of two bins, say, 12 and 13, would not have twice the amount of drop radii (not drops themselves) than each of them.

Figure 6 summarizes this feature in terms of the cumulative distribution function $F(r)$ of drop radii (appendix B). For the ensemble, the drop radii all have equal probability of occurrence; that is, the probability $F(r + \Delta r) - F(r)$ to observe a drop radius in the interval $[r + \Delta r, r)$ is proportional to its length Δr. For drops
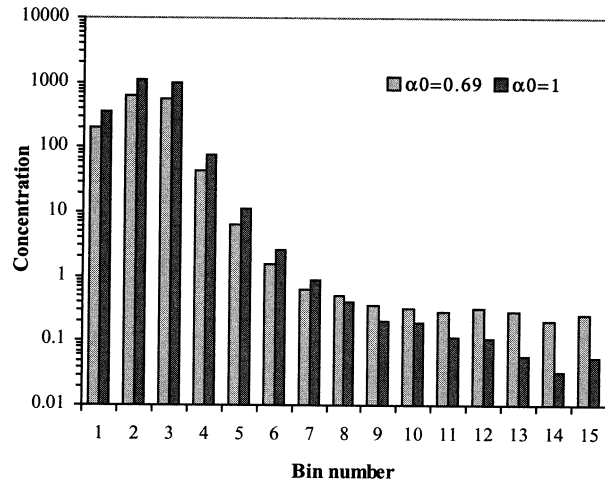
FIG. 7. Drop spectra calculated for $\alpha_0 = 0.69$ and $\alpha_0 = 1$.

above 14 μm, this probability is given by a nonlinear function, indicating that the *drop radii are not equally weighted.* The sparsity of these drops causes jumps in $F(r)$ that are clearly seen in Fig. 6. The point $r_E \approx 14$ μm at which the cumulative function $F(r)$ turns into its nonlinear part coincides with the radius of the largest drop in the ensemble. Indeed, all drop sizes between r_0 and r_E are present in every elementary volume. The probability that drops with only these radii reside in the elementary volume is given by $\alpha_0 = F(r_E) = 0.69$. In other words, α_0 is the probability that the elementary volume contains the ensemble of drops.

Note, that the cumulative distribution function $F(r)$ describes the probability of values that drop radii can take on and depends only on the binary structure of the FSSP records. However, the ensemble-based approach neglects this information, assuming that $F(r)$ is always a linear function; that is, possible values of the drop radius are uniformly distributed.

Having $F(r)$ defined, we are able to correctly answer the following question. How many drops per drop radius do appear in the 32-cm³ volume? This is given by a drop spectrum $\overline{c}(r)$, that is, the total number of drops with radii between r and $r + \Delta r$ in a unit volume normalized by the probability $F(r + \Delta r) - F(r)$ to observe a drop radius in this interval. For the ensemble, drop radii are uniformly distributed within the interval of their variation and thus the normalization factor is proportional to Δr. This does not hold true for "large drops" $(r > r_E)$; for these drops, the normalization factor varies in a nonlinear fashion (Fig. 6).

How is the drop spectrum calculated in the framework of the ensemble approach? This concept postulates that radii of the largest drop in the ensemble and the largest measured drop coincide; that is, $r_E = r_{\max}$. In other words, $F(r)$ is artificially replaced with a linear function. All drop sizes are assumed to be present in the elementary volume with a unit probability in this case; that is, $\alpha_0 = F(r_{\max}) = 1$. Figure 7 demonstrates drop spectra

$\overline{c}(r)$ calculated for both $\alpha_0 = 0.69$ and $\alpha_0 = 1$. One can see that the ensemble assumption ($\alpha_0 = 1$) has led to the misrepresentation of the "true" drop distribution ($\alpha_0 = 0.69$); it underestimates the concentration of large drops due to the overestimation of small drop concentration. The true spectrum characterizes the number of drops per drop radii *actually* present in the elementary volume, while the ensemble-based spectrum accounts for large drops *artificially* included in much smaller concentrations in every elementary volume.

Figure 8 shows the cumulative drop distribution function $N(r)$ for a mean elementary volume of 32 cm³ for which the number concentration was about 169 drops per cubic centimeter. This distribution is given by (appendix B)

$$N(r) = \alpha_0 \int_{r_0}^{\min(r, r_E)} \frac{\overline{c}(r')}{r_E - r_0} \, dr'$$

$$+ (1 - \alpha_0) \sum_{\substack{\text{all } i \leq N_{\text{bins}} \\ \text{for which } r_E \leq r_i < r}} \overline{c}(r_i) q_i, \qquad 0 \leq \alpha_0 \leq 1,$$

$$\tag{10}$$

where the coefficients q_i, $\Sigma \, q_i = 1$, are probabilities that drops of radius $r_i \geq r_E$ will appear in the direction of photon travel. One can see that $N(r)$ consists of two parts: the first one $(r < 14 \ \mu\text{m})$ *can* be approximated accurately by a continuous function, while the second one *cannot* be. The latter part is enlarged in Fig. 8b, where the discreteness is evident. This discreteness is intrinsic to the 32-cm³ volume; averaging many such volumes together cannot change the sparsity of larger drops.

If $\alpha_0 < 1$, the use of the ensemble approach alone leads to the incorrect description of the statistical properties of drop sizes. Our data analysis has shown that $r_E \approx 14$ μm; that is, drops of radii less than about 14 μm can be attributed to the ensemble of particles. The coefficient α_0 was estimated to be $\alpha_0 \approx 0.69$; that is, about 69% of all possible drop sizes are present in every elementary volume. Drops of radii from the interval $[r_0, r_E]$ made up 99.8%–99.9% of the total number of the drops registered by the FSSP. Therefore, the ensemble approach excludes only about 0.1%–0.2% of drops, in this case study.

To summarize the data analysis section, Eq. (10) was derived using an additional information on the binary structure of measured drop size distributions. The binary representation allowed us to separate continuous and discrete parts of the cumulative drop size distribution. Now substituting (10) into (1), and (1) into (2), one can derive a correct equation that describes photon interaction with a mean elementary volume of 32 cm³, for which the number concentration was about 169 drops per cubic centimeter. Based on the theory of Schwarz distributions (Richtmyer 1978), this derivation in the general case of three-dimensional absorbing and scattering media is presented in appendix C.
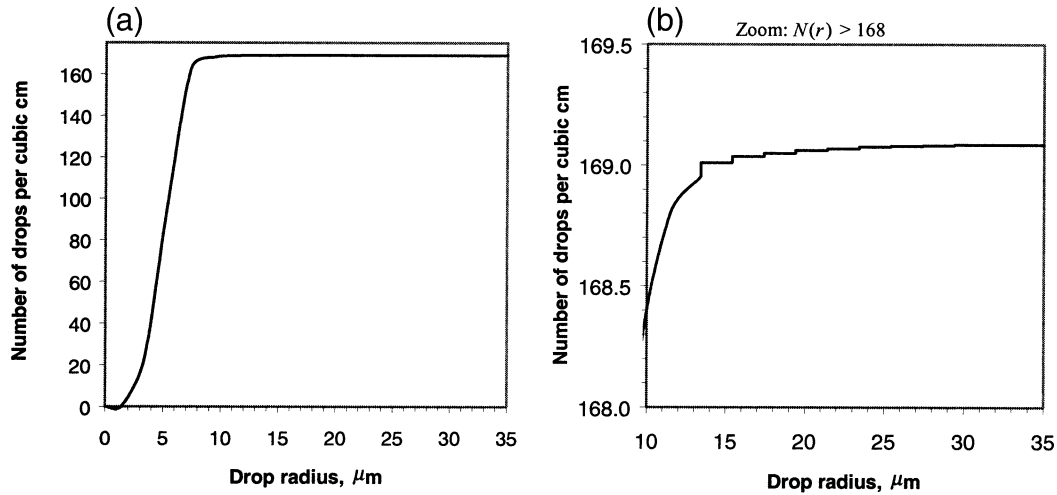
FIG. 8. (a) Cumulative drop size distribution function $N(r)$ derived from data shown in Fig. 4. This function is a weighted sum of two components. The first one continuously varies in the interval between 1.4 μm and 12 μm and describes the drop size distribution of the ensemble of particles. (b) Enlarged portion of (a) showing the second component ($r \geq 12$ μm). The second component accounts for single drops that appear randomly in the direction of photon traveling with a certain probability. The magnitudes of the jumps are determined by the probabilities p_i (Fig. 5b) of drop appearances.

4. Cloud forcing ratio

One way to look at cloud absorption in a dimensionless way is the ratio $R = C_S/C_T$, where C_S and C_T are the shortwave cloud forcing at the surface and at the top of the atmosphere, respectively. The cloud forcing is the difference between cloudy sky and clear sky net shortwave flux density (in W m^{-2}). Though R is not a direct measure of cloud absorption, it indicates the effect of clouds on column absorption. Observations collected by Cess et al. (1995), Ramanathan et al. (1995), and Pilewski and Valero (1995) estimate values of R near 1.5 while the ensemble-based radiative transfer algorithms find R about 1 (e.g., Li and Moreau 1996). Based on results of section 2 and appendix C, an analysis of the discrepancy between ensemble-based models and measurements is presented in this section. We will show that the correct treatment of drops that yields an addition of extra terms, as in Eqs. (9) and (C6), rather than the modification of the extinction coefficient, as in Eq. (8), may cause an enhanced value of R.

Consider a sufficiently extended atmospheric column bounded below by a black surface. This column represents either clear or cloudy atmosphere. We assume that the ensemble concept is able to describe scattering and absorption properties of the clear atmosphere. We idealize the cloudy atmosphere as a medium shown in Fig. 2 that consists of densely distributed small drops (gray area) and M large drops (black dots). Let the atmospheric column be illuminated by a parallel solar beam of intensity i_0 and in the direction $\mathbf{\Omega}_0$. We use the boundary value problem (C1)–(C2) for the three-dimensional transport equation to describe the radiative regime in this medium. Its solution $J(\mathbf{x}, \mathbf{\Omega})$ can be represented as (appendix C)

$$J(\mathbf{x}, \mathbf{\Omega}) = J_E(\mathbf{x}, \mathbf{\Omega}) + \sum_{k=1}^{M} J_P(\mathbf{x}, \mathbf{\Omega}, \mathbf{x}_k). \quad (11)$$

Here, J_E describes the three-dimensional radiation field due to photon interaction with the ensemble of particles and is nonresponsive to the presence of the individual drops ("black dots"), and $J_P(\mathbf{x}, \mathbf{\Omega}; \mathbf{x}_k)$ is the singular solution to the transport equation [see (C4)–(C5)] where $\mathbf{x}_k$ denotes the location of the ith black dot. The solution $J(\mathbf{x}, \mathbf{\Omega})$ is assumed to be a true radiation field in a cloudy atmosphere and the one provided by measurements while the component $J_E(\mathbf{x}, \mathbf{\Omega})$ is the ensemble-based model estimate. It should be noted that J_E ignores interaction with large drops. However, their effect to total atmospheric column absorptivity evaluated on the basis of the ensemble concept is estimated to be about 2% for large drops and 3% for very large drops (Wiscombe et al. 1984; Table 2 in Wiscombe and Welch 1986).

Note that an increase in the number M in Eq. (11) changes the sparsity of large drops. As a result, part of them will behave as the ensemble and the number of drops excluded from the ensemble will be consequently reduced. This increases the contribution of the ensemble component $J_E(\mathbf{x}, \mathbf{\Omega})$ into $J(\mathbf{x}, \mathbf{\Omega})$ via the modification of the extinction coefficient. This process sets a limit to M and, as a consequence, to the impact of the singular solution to the cloud radiation regime. The total number of large drops in Eq. (11) cannot be very high.

Let $C_{E,S}(\mathbf{\Omega}_0)$ and $C_{E,T}(\mathbf{\Omega}_0)$ be the cloud forcing at the surface level and at the top of the column, respectively, evaluated with the classical solution $J_E(r, \mathbf{\Omega})$ of the three-dimensional transport equation. We have

$$C_{E,S} = -i_0 |\mu_0| [t_E(A) - t_E(C)].$$

Here, μ_0 is the cosine of the solar polar angle, $i_0|\mu_0|$ is the downward flux density at the top of the atmosphere, and $t_E(A)$ and $t_E(C)$ are transmittances of the clear and cloudy atmospheres, respectively. Further,

$$C_{E,T} = -i_0|\mu_0|\rho, \tag{12}$$

where ρ is the difference between the reflectances of the cloudy and clear columns. In terms of these notations, the ratio between cloud forcing at the surface and the top of the atmosphere takes the form

$$R_E = \frac{C_{E,S}}{C_{E,T}} = \frac{t_E(A) - t_E(C)}{\rho}. \tag{13}$$

It follows from (11) that

$$S \cdot C_S = S \cdot C_{E,S} + i_0|\mu_0| \sum_{k=1}^{M} t_{P,k},$$

$$S \cdot C_T = S \cdot C_{E,T} + i_0|\mu_0| \sum_{k=1}^{M} (t_{P,k} + a_{P,k}). \tag{14}$$

Here, S is an area of the column upper (lower) boundary, $t_{P,k}$ (in m²) and $a_{P,k}$ (in m²) are the downward flux (in W) at the surface level, and the column absorption (in W) resulted from the singular component $J_P(\mathbf{x}, \boldsymbol{\Omega}; \mathbf{x}_k)$ normalized by the incident flux density $i_0|\mu_0|$ (in W m⁻²). It should be emphasized that the singular component $J_P(\mathbf{x}, \boldsymbol{\Omega}; \mathbf{x}_k)$ contains the delta function $\delta[\boldsymbol{\Omega} - (\mathbf{x} - \mathbf{x}_k)/|\mathbf{x} - \mathbf{x}_k|]$, which relates directions and spatial points (appendix C). Its integration over S (or over the whole column) does not result in a value proportional to S; that is, $t_{P,k}$ and $a_{P,k}$ are bounded functions with respect to the area S of the column lower boundary.

Let $\bar{t}$ and $\bar{a}$ be the mean normalized downward flux and the mean normalized column absorption of individual drops excluded from the ensemble:

$$\bar{t} = \frac{1}{M} \sum_{k=1}^{M} t_{P,k}, \qquad \bar{a} = \frac{1}{M} \sum_{k=1}^{M} a_{P,k}. \tag{15}$$

It follows from (12)–(15) that

$$S \cdot C_S = S \cdot C_{E,S} + i_0|\mu_0|M\bar{t} = S \cdot R_E C_{E,T} + i_0|\mu_0|M\bar{t}$$

$$= -S \cdot R_E i_0|\mu_0|\rho + i_0|\mu_0|M\bar{t};$$

$$S \cdot C_T = -S \cdot i_0|\mu_0|\rho + i_0|\mu_0|M(\bar{t} + \bar{a}).$$

Thus, the model estimates $R_E = C_{E,S}/C_{E,T} \approx 1$, while the measurements provide

$$R(M) = \frac{C_S}{C_T} = \frac{S \cdot R_E\rho - M\bar{t}}{S \cdot \rho - M(\bar{t} + \bar{a})}. \tag{16}$$

Let us discuss this equation. The ratio $R(M)$ is an increasing function with respect to M when $R_E > \bar{t}/(\bar{t} + \bar{a})$. If $M = 0$, then $R(0) = R_E$. It has a vertical asymptote, $M = S\rho/(\bar{t} + \bar{a})$, and a horizontal asymptote, $R = \bar{t}/(\bar{t} + \bar{a})$. If clouds do not absorb the intercepted radiation (i.e., $\bar{a} = 0$) and $R_E = 1$, R becomes insensitive to the presence of individual drops and takes on the

value 1. However, the absorbing medium ($\bar{a} > 0$) can, potentially, result in any value of R between R_E ($M = 0$) and infinity [$M(\bar{t} + \bar{a}) = S\rho$]. While this is true mathematically, the natural conditions under which R would be significantly greater than R_E are not met. For example, the vertical asymptote $M(\bar{t} + \bar{a}) = S\rho$ means that the net shortwave flux of radiation reflected by M individual drops is equal to the cloud forcing at the top of the atmosphere resulted from an ensemble of drops. To achieve this, the total number of large drops should be comparable with the column volume. In this case, at least part of large drops should be attributed to the ensemble. This leads to fewer drops being excluded from the ensemble, and thus the ratio $R(M)$ does not take an infinite value. From the other side, if the concentration of large drops is small, their contribution to $R(M)$ is not significant either. Increasing the number of large drops leads to a smaller concentration of drops excluded from the ensemble. Thus, again, the total contribution of single drops to the ratio $R(M)$ will not be large. However, there is an intermediate case when the number of large drops is not small enough to be neglected, and not large enough to be attributed to the ensemble. An accurate analysis of physical constraints on $R(M)$ is the topic of a special investigation, and will not be discussed here. Here, based on Eq. (16), we show that a reasonable number of single drops may be enough to increase the ratio $R(M)$ to 1.5 [as reported in the literature for at least the warm pool (Ramanathan and Vogelmann 1997)].

Let n be the concentration of drops excluded from the ensemble defined as the ratio between the total number M of large drops in the column to the column volume SH. Here, H is the column height. Solving Eq. (16) for M and accounting for $n = M/SH$ yields

$$n = \rho H^{-1} \frac{R - R_E}{(R - 1)\bar{t} + R\bar{a}}.$$

We take $R = 1.5$ while $R_E = 1$. Cloudy and cloudless atmospheres reflect 30% and 13% of the incoming radiation, respectively (Liou 1992, 11–12); that is, $\rho = 0.30 - 0.13 = 0.17$. For the optically thick cloud $\bar{t} \approx 0$; that is, the normalized downward flux of photons from the incident radiation that are scattered by individual drops and reach the surface without experiencing another collision is small. The normalized absorption $\bar{a}$ is the mean fraction of energy incident on large drops that the drops absorb plus the mean fraction of energy scattered by the large drops that the ensemble of particles absorbs. The effect of large drops to total atmospheric column absorptivity evaluated on the basis of the ensemble concept is about 3% (Wiscombe et al. 1984; Wiscombe and Welch 1986). Although this could be an underestimation of the true absorption, it can be taken as a lower bound of $\bar{a}$; that is, $\bar{a} \gtrsim 0.03$. Assuming the cloud height $H = 1$ km $= 10^5$ cm, one obtains

$$n = 0.17 \times 10^{-5} \frac{1}{t + 3\overline{a}} \leq 1.9 \times 10^{-5}.$$

This is consistent with the number concentration of 30-μm and larger drops obtainable from the model of normal drop size distribution (see Fig. 1 in Wiscombe et al. 1984). In other words, a reasonable concentration number of large drops, if treated correctly, might be plausible to explain the enhanced ratios of the shortwave cloud forcing reported in the literature.

5. Conclusions

Radiative transfer in clouds is described by the radiative transfer equation. In this equation, scattering and absorption properties of an ensemble of cloud drops are characterized by a drop size density distribution function (Liou 1992, p. 255). The notion of ensemble is based on the assumption that an elementary volume has either all drop sizes (as in clouds) or no drops at all (as in gaps between clouds). A realistic cloud contains a huge number of small drops and a tiny number of large ones. It is clear that large drops cannot be present in every elementary volume. In other words, the ensemble concept fails to account for large drops being rare in occurrence.

Attempts were made to include the large (and very large) drops into the classical radiative transfer (Welch et al. 1980; Wiscombe et al. 1984; Wiscombe and Welch 1986). How differently does classical radiative transfer theory treat cases with and without large drops? To build a cloud drop size density distribution function, drops excluded from the ensemble are distributed uniformly over the space. They are artificially fractionated (included in concentrations less than one per elementary volume) even though this is obviously a poor assumption since drops are discrete. As a result, a new extinction coefficient is defined; obviously, it is bigger than the one that ignores the large drops. This results in a positive increment in cloud absorption. Solution of the transport equation continuously depends on the extinction coefficient. This means that the increment in cloud absorption degrades continuously as soon as the concentration of large drops tends to zero. The main conclusion from these studies is that large and even very large drops do not yield enough increase in cloud absorption to explain recently found discrepancies between models and measurements (e.g., Valero et al. 2000).

The data analysis presented in section 3 points to the presence of jumps in the cumulative drop size distribution whose magnitudes are related to the frequencies of large drop occurrence. This makes it impossible to use the density distribution function for characterizing the variation in drop sizes without a loss of information. We showed that if the drop size distribution is treated properly, an additional component, the Green's function, must be added to the solution of the radiative transfer equation (section 2). The true solution is thus a sum of two components that represent contributions from the ensemble of particles and from large single drops (appendix C). There are two different mechanisms involved in the accumulation of energy absorbed by drops. The first one is the integration of radiance over the photon path: the longer the photon path is, the higher the amount of absorbed energy. The second one sums jumps in the true solution, each corresponding to a photon path of length zero. This enhances the absorption with the photon path unchanged. The ensemble assumption excludes the latter case and thus may lead to the discrepancies between the ensemble-based models and measurements. More research is needed to quantitatively address this question. However, as was shown in this paper (section 4), the correct interpretation of large drops might be plausible to explain the enhanced values of the ratio between the shortwave cloud forcing at the surface and at the top of the atmosphere reported in literature (e.g., Ramanathan and Vogelmann 1997).

APPENDIX A

Derivation and Solution of Eq. (7)

Let $\varphi(x)$ be a continuous function. The following formula is required to derive Eq. (7):

$$\int_a^b \varphi(x) \, d\mathcal{H}(x - x_0) = \varphi(x_0). \tag{A1}$$

Here, $\mathcal{H}(x - x_0)$ is the Heaviside function, which is equal to 1 if $x > x_0$, and 0 otherwise; and (A1) is the Lebesgue–Stieltjes integral (Richtmyer 1978). This formula justifies that $d\mathcal{H}(x - x_0)/dx = \delta(x - x_0)$, where $\delta(x)$ is the Dirac delta function.

Substituting (6) into (1) and accounting for (A1), one obtains

$$d\tau(\xi) = \int_0^\infty \sigma_{\text{ext}}(r) \, d_r \{ [C(r, \, \xi + d\xi) - C(r, \, \xi)] $$
$$+ [\mathcal{H}(\xi + d\xi - \xi_1)\mathcal{H}(r - r_{\text{E}}) $$
$$- \mathcal{H}(\xi - \xi_1)\mathcal{H}(r - r_{\text{E}})] \}$$

$$= \int_0^\infty \sigma_{\mathrm{ext}}(r)\frac{d^2C(r,\ \xi)}{drd\xi}\ dr\ d\xi$$

$$+ \int_0^\infty \sigma_{\mathrm{ext}}(r)\ d\mathcal{H}(r - r_{\mathrm{E}})\ d\mathcal{H}(\xi - \xi_1)$$

$$= \sigma_{\mathrm{E}}d\xi + \sigma_{\mathrm{ext}}(r_{\mathrm{E}})d\mathcal{H}(\xi - \xi_1),$$

where σ_{E} is defined by (4), and $c(r,\ \xi) = d^2C(r,\ \xi)/dr\ d\xi$ is the probability density distribution function. Equation (7) can now be obtained by substituting $d\tau(\xi)$ into (2).

Let $\xi < \xi_1$ or $\xi \geq \xi_1 + \varepsilon$, where ε is a sufficiently small positive number. The term $d\mathcal{H}(\xi - \xi_1)$ vanishes and Eq. (7) takes the form $dI(\xi) + \sigma_{\mathrm{E}}I(\xi)d\xi = 0$. Its solution is $I(\xi) = i_0 \exp(-\sigma_{\mathrm{E}}\xi)$, if $\xi < \xi_1$, and

$$I(\xi) = I(\xi_1 + \varepsilon) \exp[-\sigma_{\mathrm{E}}(\xi - \xi_1 - \varepsilon)], \quad \text{(A2)}$$

if $\xi \geq \xi_1 + \varepsilon$.

Let $\xi_1 \leq \xi < \xi_1 + \varepsilon$. It follows from the equalities $dI(\xi_1) = I(\xi_1 + \varepsilon) - I(\xi_1)$ and $d\mathcal{H}(\xi_1 - \xi_1) = \mathcal{H}(\xi_1 + \varepsilon - \xi_1) - \mathcal{H}(\xi_1 - \xi_1) = 1$ that $I(\xi_1 + \varepsilon) - I(\xi_1) + \sigma_{\mathrm{E}}I(\xi_1)\varepsilon + \sigma_{\mathrm{ext}}(r_{\mathrm{E}})I(\xi_1) = 0$. Tending ε to zero results in

$$I^-(\xi_1) - I^+(\xi_1) = \sigma_{\mathrm{ext}}(r_{\mathrm{E}})I^-(\xi_1), \quad \text{(A3)}$$

where $I^\pm(\xi_1)$ are the limits of $I(\xi_1 \pm \varepsilon)$ as ε tends to zero. Solving Eq. (A3) for $I^+(\xi_1)$ and substituting $I^+(\xi_1)$ into (A2), one obtains the solution to Eq. (7):

$$I(\xi) = \begin{cases} 0, & \xi < 0; \\ i_0 \exp(-\sigma_{\mathrm{E}}\xi), & 0 \leq \xi < \xi_1; \\ [1 - \sigma_{\mathrm{ext}}(r_{\mathrm{E}})]i_0 \exp(-\sigma_{\mathrm{E}}\xi), & \xi \geq \xi_1. \end{cases}$$
$$\text{(A4)}$$

APPENDIX B

Derivation of the Cumulative Distribution Function

Probability theory starts with the definition of a simple event. The event "drops of radius η_r appear in the elementary volume with concentration η_c" is taken as the simple event. A concentration is defined here as the number of drops in an elementary volume of 32 cm³ normalized by 32 cm³. We depict the simple event as a point $\eta = (\eta_r, \eta_c)$ on a plane with random variables η_r and η_c. This plane is the sample space. A point $\eta = (\eta_r, 0)$ signifies that the drop does not appear in the elementary volume. The appearance of drop radii along the horizontal axis, therefore, is given by a *conditional probability* $F(r)$ of the event $\eta_r < r$, given that $\eta_c \neq 0$. We start our analysis with the derivation of $F(r)$.

The sample space is composed of $15 \times 98 = 1470$ simple events $\eta = [r_i, c_{\mathrm{obs},k}(r_i)]$; $i = 1, 2, \ldots, 15$; $k = 1, 2, \ldots, 98$. Here 15 and 98 are numbers of the FSSP bins N_{bins} and the selected records N_{rec}, respectively, and $c_{\mathrm{obs},k}(r_i)$ is the concentration of drops registered by the ith FSSP bin. We assume that the random variable η_r is uniformly distributed along the horizontal axis of the sample space. Let H_i be the event "the random variable η_r has taken on a value in the ith FSSP bin." This event is represented by the interval $[r_{i-1}, r_i)$. The number of different η_r observed in this interval is proportional to Δr. We denote by B the event "$\eta_c \neq 0$." In the sample space, this event is represented by points $\eta = (\eta_r, \eta_c)$, which do not lie on the horizontal axis $c = 0$. Its probability can be calculated as the ratio of the number of "black rectangles" in Fig. 5a to the total number of "rectangles." For the selected data, $P(B) = 0.57$. It means that the distribution $F(r)$ should describe how 57% of the points from the interval $[r_0, r_{\mathrm{max}}]$ are distributed within this interval.

The probability $F(r + \Delta r) - F(r)$ to observe a drop radius in the interval $[r, r + \Delta r)$ is given by the conditional probability $P(H_i|B)$ of the event H_i under the condition B; that is,

$$F(r_{i-1} + \Delta r) - F(r_{i-1}) = \frac{P(B \cap H_i)}{P(B)}$$

$$= \frac{P(B \cap H_i)}{\sum\limits_{k=1}^{N_{\mathrm{bins}}} P(B \cap H_k)}. \quad \text{(B1)}$$

For drop radii that appear in the FSSP bin with a unit probability (see Fig. 5b), H_i is a subset of B; that is, $H_i \subset B$. The event $B \cap H_i$, therefore, is represented by the interval $[r_{i-1}, r_i)$, and its probability is proportional to its length Δr. The ensemble approach assumes that this property holds true independently of the bin width Δr. For large drops, the event $B \cap H_i$ can be represented by an infinitesimal interval, while the probability of $B \cap H_i$ takes on a finite number. The probability, therefore, cannot be associated with Δr; but instead with Δr^{D_i}, where $0 \leq D_i \leq 1$ is the Hausdorf–Besicovitch dimension of the set $B \cap H_i$ (Barnsley 1993; Federer 1969). For bins with a unit probability (Fig. 5b), $D_i = 1$ and $P(B \cap H_i)$ is proportional to Δr. For large drops, the Hausdorf–Besicovitch dimension can fall below unity, and thus $P(B \cap H_i)$ is proportional to Δr^{D_i}. Let $p_i(\Delta r)$ be the coefficient of proportionality. In terms of these notations, (B1) can be written as

$$F(r_{i-1} + \Delta r) - F(r_{i-1}) = \frac{p_i(\Delta r)\Delta r^{D_i}}{\sum\limits_{k=1}^{N_{\mathrm{bins}}} p_k(\Delta r)\Delta r^{D_k}}. \quad \text{(B2)}$$

The coefficient $p_i(\Delta r)$ is the probability of the event $\eta_c \neq 0$, given that $r_{i-1} \leq \eta_r < r_{i-1} + \Delta r$; that is, $p_i(\Delta r) = P(B | H_i)$. Their values are shown in Fig. 5b. It follows from (B2) that the probability density distribution function dF/dr at r_{i-1} can be defined if and only if $D_i = 1$.

Consider a set of all simple events for which $p_i(\Delta r) = 1$. This set separates drop radii that appear in the elementary volume with a unit probability; that is, those drops to which the concept of the ensemble is applicable.

The Hausdorf–Besicovitch dimension is unity in this case. For sufficiently large drops, the bin width $\Delta r = 2$ μm can be treated as a infinitesimal interval in comparison with the drop radius. Their appearance in a 2-μm interval, therefore, can be treated as a discrete random variable; that is, $D_i = 0$. There is an intermediate case when drops are not small enough to densely fill the interval $[r_{i-1}, r_{i-1} + \Delta r)$, and not large enough to be treated as a discrete variable. Theoretically, the Hausdorf–Besicovitch dimension can take any value between 0 and 1. Our data do not provide enough information to analyze this case. We assume that D_i can take on two values only, that is, 1 if $p_i(\Delta r) = 1$, and zero otherwise. Based on this assumption, the radius r_E of the largest drop in the ensemble coincides with the largest edge of the FSSP bin for which $p_i(\Delta r) = 1$. For the selected data, $r_E \approx 14$ μm. The probability α_0 that the elementary volume contains the ensemble of drops can be evaluated as

$$\alpha_0 = \frac{\displaystyle\sum_{\text{all } i \text{ for which } D_i = 1} p_i(\Delta r)\Delta r}{\displaystyle\sum_{k=1}^{N_{\text{bins}}} p_k(\Delta r)\Delta r^{D_k}}$$

$$= \frac{r_E - r_0}{r_E - r_0 + \displaystyle\sum_{\text{all } k \text{ for which } D_k = 0} p_k(\Delta r)}.$$

We split the sums in Eq. (B2) into two sub-sums, which include summands $D_i = 1$ and $D_i = 0$, respectively. This allows us to express $F(r)$ as

$$F(r) = \alpha_0 F_0(r) + (1 - \alpha_0)\Phi(r). \tag{B3}$$

Here, $F_0(r)$ is cumulative distribution function of the ensemble of drops:

$$F_0(r) = \frac{\displaystyle\sum_{\text{all } i \text{ for which } D_i = 1 \text{ and } r_i < r} \Delta r}{\displaystyle\sum_{\text{all } k \text{ for which } D_k = 1} \Delta r} = \frac{r - r_0}{r_E - r_0},$$

if $r_0 \leq r < r_E$; and $F_0(r) = 0$, if $r \leq r_0$ or $r > r_E$. The second component can be expressed as

$$\Phi(r) = \sum_{\text{all } i \text{ for which } r_i < r} q_i.$$

Here,

$$q_i = \frac{p_i(\Delta r)}{\displaystyle\sum_{\text{all } k \text{ for which } D_k = 0} p_k(\Delta r)},$$

if $p_i(\Delta r) < 1$, and 0 otherwise. The distribution $\Phi(r)$ is the cumulative distribution function of drops excluded from the ensemble. If $\alpha_0 = 1$, then $F(r + \Delta r) - F(r) = \Delta r/(r_{\max} - r_0)$; that is, the number of drop radii in the interval $[r, r + \Delta r)$ is proportional to its length Δr. The probability density distribution function can be used in this case. Figure 6 demonstrates the distribution (B3) derived from data used in this study.

The drop spectrum $\overline{c}(r)$ can be calculated as

$$\overline{c}(r_i) = \frac{\dfrac{1}{N_{\text{rec}}} \displaystyle\sum_{k=1}^{N_{\text{rec}}} c_{\text{obs},k}(r_i)}{F(r_i) - F(r_{i-1})}.$$

Examples of this function for $\alpha_0 = 0.69$ and $\alpha_0 = 1$ are shown in Fig. 7. Note that the ensemble approach ($\alpha_0 = 1$) underestimates the contribution of large drops.

The cumulative drop size distribution $N(r)$ can be expressed as

$$N(r) = \int_{r_0}^{r} \overline{c}(r) \, dF(r). \tag{B4}$$

Substituting (B3) into (B4), one obtains (10).

APPENDIX C

Radiative Transfer in Three-Dimensional Cloud

Consider the three dimensional medium shown in Fig. 2. We use the boundary value problem for the three dimensional transport equation to describe radiative transfer in this medium, which is assumed to be bounded from below and on lateral sides by an absorbing surface

$$\mathbf{\Omega} \cdot \nabla J(\mathbf{x}, \mathbf{\Omega}) + \chi(\mathbf{x})J(\mathbf{x}, \mathbf{\Omega})$$

$$= \frac{\chi_s(\mathbf{x})}{4\pi} \int_{4\pi} J(\mathbf{x}, \mathbf{\Omega}') \, d\mathbf{\Omega}', \tag{C1}$$

$$J(\mathbf{x}_t, \mathbf{\Omega}) = i_0\delta(\mathbf{\Omega} - \mathbf{\Omega}_0), \qquad \mathbf{n}_t \cdot \mathbf{\Omega} < 0,$$

$$J(\mathbf{x}_b, \mathbf{\Omega}) = 0, \qquad \mathbf{n}_b \cdot \mathbf{\Omega} < 0. \tag{C2}$$

Here, χ takes on values σ_E and $\sigma_{\text{ext}}(r_E)$ at the "gray" and "black" dots, where σ_E and σ_{ext} are the extinction coefficient and the particle extinction cross section, respectively. The function χ_s describes scattering properties of the ensemble of particles and individual drops. This is a two-value function: $\chi_s(\mathbf{x}) = \sigma_{E,s}$ if $\mathbf{x}$ belongs to the gray area, and $\chi_s(\mathbf{x}) = \sigma_s(r_E)$ otherwise; $\sigma_{E,s}$ and $\sigma_s(r_E)$ are the scattering coefficient for the ensemble of drops and the particle scattering cross section, respectively. Symbols $\mathbf{x}_t$ and $\mathbf{x}_b$ denote points on the top (subscript "t"), bottom, and lateral (subscript "b") boundaries; $\mathbf{n}_t$ and $\mathbf{n}_b$ are outward normals to the boundary at $\mathbf{x}_t$ and $\mathbf{x}_b$, respectively; i_0 is the intensity of the incident beam; and the bold raised dot denotes the scalar product. For ease of analysis, we assume that there is one individual drop of radius r_E at the point $\mathbf{x}_0 + \xi_1\mathbf{\Omega}_0$, where $\mathbf{x}_0$ is a point on the upper medium boundary $z = 0$. Note that the choice of an isotropic phase function in Eq. (C1) is not essential here and it has been assumed only for simplicity.

The solution $J(r, \mathbf{\Omega})$ to this problem is the radiance at $\mathbf{x}$ in the direction $\mathbf{\Omega}$, which is treated as a Schwartz distribution. Schwartz theory distinguishes two types of functions: regular and singular distributions (Vladimirov 1971). There is a one-to-one correspondence between "usual functions" and regular distributions, and thus, an ordinary function can be regarded as a special case of a

distribution. The Dirac delta function is the simplest example of a singular distribution. No usual function can be identified with it (Vladimirov 1971). In general, a solution of the transport equation can be expressed as a sum of regular and singular distributions. The singular summand must be separated explicitly because numerical technique cannot deal with singular distributions. The mathematical theory of Schwartz distributions applicable to the transport equation was developed by Germogenova (1986). Choulli and Stefanov (1996) and Antyufeev and Bondarenko (1996) recently reported that there is a one-to-one correspondence between the complicated three-dimensional structure of the medium and radiation exiting the medium. An additional singular distribution in the solution of the three-dimensional transport equation makes this one-to-one correspondence possible. Zhang et al. (2002) showed that the singular solution to the transport equation is responsible for the hot spot effect, that is, a sharp peak in radiation reflected by the vegetation canopy in the retrosolar direction that is neglected by classical radiative transfer. Below we will closely follow the ideas of Germogenova (1986), Choulli and Stefanov (1996), Antyufeev and Bondarenko (1996), and Zhang et al. (2002).

Photons entering the medium through the point $\mathbf{x}_0$ on the upper boundary in the direction $\mathbf{\Omega}_0$ and being attenuated by the ensemble of particles experience the first collision at the point $\mathbf{x}_0 + \xi_1\mathbf{\Omega}_0$, which results in the appearance of a point diffuse source. It is intuitively clear that the three-dimensional radiation field decomposes into two very different fields (Fig. 2). The first field is generated by a diffuse source at $\mathbf{x}_0 + \xi_1\mathbf{\Omega}_0$, and the second one comes from photons penetrating into the medium through elementary surfaces on the upper boundary that exclude $\mathbf{x}_0$. The incident beam, therefore, should be treated as a horizontally inhomogeneous field with respect to its contribution to the radiation regime inside the medium. We treat each point on the upper boundary as a point monodirectional source and formulate the radiative transfer problem for each such source. The radiative response of the medium at $\mathbf{x}$ in direction $\mathbf{\Omega}$ to a point monodirectional source located at $\mathbf{x}_0$ is the Green's function, $G(\mathbf{x}, \mathbf{\Omega}; \mathbf{x}_0, \mathbf{\Omega}_0)$ (Bell and Glasstone 1970), which satisfies Eq. (C1), and where $G(\mathbf{x}_t, \mathbf{\Omega}; \mathbf{x}_0, \mathbf{\Omega}_0) = \delta(\mathbf{x}_t - \mathbf{x}_0) \cdot \delta(\mathbf{\Omega} - \mathbf{\Omega}_0)$. The so-

lution to the problem [Eqs. (C1)–(C2)] can be expressed as an integral over the upper surface $z = 0$ of the Green's function as

$$J(\mathbf{x}, \mathbf{\Omega}) = i_0 \int G(\mathbf{x}, \mathbf{\Omega}; \mathbf{x}_0, \mathbf{\Omega}_0)|\mathbf{n}_t \cdot \mathbf{\Omega}_0|\, dS. \quad \text{(C3)}$$

A technique to separate the singular components from Eq. (C3) is based on the following result (Germogenova 1986; Choulli and Stefanov 1996): for a three-dimensional medium, radiances G_0 and G_1 of uncollided and single scattered photons from a point monodirectional source are singular distributions, while the remaining field is described by a regular distribution G_R. The Green's function, therefore, is the sum of two singular and one regular component; that is, $G = G_0 + G_1 + G_R$. Substituting this sum into Eq. (C3) results in the decomposition of the solution $J(r, \mathbf{\Omega})$ into three terms, $J = J_0 + J_1 + J_R$, which are integrals over the upper boundary of G_0, G_1, and G_R, respectively. Because G_R is a regular function, the third integral J_R is insensitive to a value of G_R at a particular point $\mathbf{x}_0$; that is, one can ignore the point $\mathbf{x}_0$ when integrating G_R over the upper boundary surface. This means that the contribution of multiply scattered photons entering the medium through the point $\mathbf{x}_0$ to the term J_R can be neglected.

The singular nature of G_0 and G_1 makes their integrals sensitive to particular points of the upper boundary. Therefore, we perform the integration Eq. (C3) over the upper boundary surface in two parts, the first excludes the point $\mathbf{x}_0$ and then separately over the point $\mathbf{x}_0$. The former separates photons "continuously" penetrating into the medium through elementary surfaces while the latter specifies the path that results in the illumination of the scattering center at $\mathbf{x}_0 + \xi_1\mathbf{\Omega}_0$ (Fig. 2). The integration of G_0 and G_1 over the surface results in similar expressions for the unscattered and once scattered radiance. Thus, the sum of J_R and these two terms is the solution J_E of the boundary value problem [Eqs. (C1)–(C2)]. Note that J_E consists of a singular (unscattered intensity) and regular (diffuse intensity) components.

The integration of G_0 and G_1 over the set of points $\{\mathbf{x}_0\}$ results in $J_P = J_{P,0} + J_{P,1}$, where (Germogenova 1986)

$$J_{P,0}(\mathbf{x}, \mathbf{\Omega}; \mathbf{x}_1) = \frac{I(|\mathbf{x} - \mathbf{x}_0|)}{|\mathbf{x} - \mathbf{x}_0|^2}\delta(\mathbf{\Omega} - \mathbf{\Omega}_0)\delta\left(\mathbf{\Omega} - \frac{\mathbf{x} - \mathbf{x}_0}{|\mathbf{x} - \mathbf{x}_0|}\right)\mathcal{H}(|\mathbf{x}_1 - \mathbf{x}_0| - |\mathbf{x} - \mathbf{x}_0|)$$

$$+ \frac{I(|\mathbf{x} - \mathbf{x}_1|)}{|\mathbf{x} - \mathbf{x}_1|^2}\delta(\mathbf{\Omega} - \mathbf{\Omega}_0)\delta\left(\mathbf{\Omega} - \frac{\mathbf{x} - \mathbf{x}_1}{|\mathbf{x} - \mathbf{x}_1|}\right)\mathcal{H}(|\mathbf{x} - \mathbf{x}_0| - |\mathbf{x}_1 - \mathbf{x}_0|); \quad \text{(C4)}$$

$$J_{P,1}(\mathbf{x}, \mathbf{\Omega}; \mathbf{x}_1) = I(|\mathbf{x}_1 - \mathbf{x}_0|)\frac{\sigma_s(r_E)\exp(-\sigma_E|\mathbf{x} - \mathbf{x}_1|)}{4\pi|\mathbf{x} - \mathbf{x}_1|^2}\delta\left(\mathbf{\Omega} - \frac{\mathbf{x} - \mathbf{x}_1}{|\mathbf{x} - \mathbf{x}_1|}\right). \quad \text{(C5)}$$

Here, $\mathbf{x}_1 = \mathbf{x}_0 + \xi_1\mathbf{\Omega}_0$, $\mathcal{H}$ is the Heaviside function, $|\mathbf{x} - \mathbf{x}_1|$ is the distance between $\mathbf{x}$ and $\mathbf{x}_1$, and I is given by (A4). Thus, a formal mathematical solution to the problem [Eqs. (C1)–(C2)] is

$$J(\mathbf{x}, \mathbf{\Omega}) = J_{\mathrm{E}}(\mathbf{x}, \mathbf{\Omega}) + J_{\mathrm{P}}(\mathbf{x}, \mathbf{\Omega}; \mathbf{x}_1). \qquad (C6)$$

The first summand J_{E} describes the three-dimensional radiation field generated by photons penetrating into the medium through elementary surfaces on the upper medium boundary and is insensitive to the presence of the individual scattering center $\mathbf{x}_1$ and the path $\mathbf{x}_0 + \xi\mathbf{\Omega}_0$. We term J_{E} the classical solution of the transport equation [Eq. (C1)]. The second summand J_{P} is the radiative response of the medium to the point source, which is a singular distribution. With changes in the number of black dots the classical solution J_{E} is unchanged but the singular component transforms to the sum of $J_{\mathrm{P}}(\mathbf{x}, \mathbf{\Omega}; \mathbf{x}_i)$ over $\mathbf{x}_i$, $i = 1, 2, \ldots, M$.

REFERENCES

Albrecht, B. A., D. A. Randall, and S. Nicholls, 1988: Observations of marine stratocumulus clouds during FIRE. *Bull. Amer. Meteor. Soc.,* **69,** 618–626.

Antyufeev, V. S., and A. N. Bondarenko, 1996: X-ray tomography in scattering media. *SIAM J. Appl. Math.,* **56,** 573–587.

Arking, A., 1996: Absorption of solar energy in the atmosphere: Discrepancy between model and observations. *Science,* **273,** 779–782.

——, 1999: The influence of clouds and water vapor on atmospheric absorption. *Geophys. Res. Lett.,* **26,** 2729–2732.

Asano, S., A. Uchiyama, Y. Mano, M. Murakami, and Y. Takayama, 2000: No evidence for solar absorption anomaly by marine water clouds through collocated aircraft radiation measurements. *J. Geophys. Res.,* **105,** 14 761–14 775.

Barker, H. W., J.-J. Morcrette, and G. D. Alexander, 1998: Broadband solar fluxes and heating rates for atmospheres with 3D broken clouds. *Quart. J. Roy. Meteor. Soc.,* **124,** 1245–1271.

Barnsley, M. F., 1993: *Fractals Everywhere.* Academic Press, 531 pp.

Bell, G. I., and S. Glasstone, 1970: *Nuclear Reactor Theory.* Van Nostrand Reinholt, 619 pp.

Bohren, C. F., and D. R. Huffman, 1983: *Absorption and Scattering of Light by Small Particles.* J. Wiley and Sons, 530 pp.

Cess, R. D., and Coauthors, 1995: Absorption of solar radiation by clouds: Observation versus models. *Science,* **267,** 496–499.

——, M. Zhang, F. P. J. Valero, S. K. Pope, A. Bucholtz, B. Bush, C. S. Zender, and J. Vitko Jr., 1999: Absorption of solar radiation by the cloudy atmosphere: Further interpretations of collocated aircraft measurements. *J. Geophys. Res.,* **104,** 2059–2066.

Choulli, M., and P. Stefanov, 1996: Reconstruction of the coefficient of the stationary transport equation from boundary measurements. *Inverse Probl.,* **12,** L19–L23.

Collins, W. D., 1998: A global signature of enhanced shortwave absorption by clouds. *J. Geophys. Res.,* **103,** 31 669–31 679.

Federer, H., 1969: *Geometric Measure Theory.* Springer-Verlag, 676 pp.

Germogenova, T. A., 1986: *The Local Properties of the Solution of the Transport Equation* (in Russian). Nauka, 272 pp.

King, M. D., L. F. Radke, and P. V. Hobbs, 1990: Determination of the spectral absorption of solar radiation by marine stratocumulus clouds from airborne measurements within clouds. *J. Atmos. Sci.,* **47,** 894–907.

——, ——, and ——, 1993: Optical properties of marine stratocumulus clouds modified by ships. *J. Geophys. Res.,* **98,** 2729–2739.

Li, Z.-Q., and L. Moreau, 1996: Alteration of solar absorption by clouds: Simulation and observation. *J. Appl. Meteor.,* **35,** 653–670.

Liou, K. N., 1992: *Radiation and Cloud Processes in the Atmosphere.* Oxford University Press, 487 pp.

Liu, Y. G., and J. Hallett, 1998: On size distributions of cloud droplets growing by condensation: A new conceptual model. *J. Atmos. Sci.,* **55,** 527–536.

Marshak, A., A. Davis, W. J. Wiscombe, W. Ridgway, and R. F. Cahalan, 1998: Biases in shortwave column absorption in the presence of fractal clouds. *J. Climate,* **11,** 431–446.

O'Hirok, W., C. Gautier, and P. Ricchiazzi, 2000: Spectral signature of column solar radiation absorption during the Atmospheric Radiation Measurement Enhanced Shortwave Experiment (ARESE). *J. Geophys. Res.,* **105,** 17 471–17 480.

Pilewski, P., and F. P. J. Valero, 1995: Direct observation of excess solar absorption by clouds. *Science,* **267,** 1626–1629.

Ramanathan, V., and A. M. Vogelmann, 1997: Greenhouse effect, atmospheric solar absorption and the earth's radiation budget: From the Arrhenius–Langley era to the 1990s. *Ambio,* **26,** 38–46.

——, B. Subasilar, G. J. Zhang, W. Conant, R. D. Cess, J. T. Kiehl, H. Grassl, and L. Shi, 1995: Warm pool heat budget and software cloud forcing: A missing physics? *Science,* **267,** 499–503.

Richtmyer, R. D., 1978: *Principles of Advanced Mathematical Physics.* Vol. 1. Springer-Verlag, 422 pp.

Stephens, G. L., 1996: How much solar radiation do clouds absorb? *Science,* **271,** 1131–1133.

——, and S.-C. Tsay, 1990: On the cloud absorption anomaly. *Quart. J. Roy. Meteor. Soc.,* **116,** 671–704.

Valero, F. P. J., P. Minnis, S. K. Pope, A. Bucholtz, B. C. Bush, D. R. Doelling, W. L. Smith, and X. Q. Dong, 2000: Absorption of solar radiation by the atmosphere as determined using satellite, aircraft, and surface data during the Atmospheric Radiation Measurement. *J. Geophys. Res.,* **105,** 4743–4758.

van de Hulst, H. C., 1981: *Light Scattering by Small Particles.* Dover, 470 pp.

Vladimirov, V. S., 1971: *Equations of Mathematical Physics.* Marcel Dekker, 418 pp.

Welch, R. M., S. K. Cox, and J. M. Davis, 1980: *Solar Radiation and Clouds. Meteor. Monogr.,* No. 39, Amer. Meteor. Soc., 96 pp.

Wiscombe, W., and R. M. Welch, 1986: Reply. *J. Atmos. Sci.,* **43,** 401–407.

——, ——, and W. D. Hall, 1984: The effect of very large drops on cloud absorption. Part I: Parcel models. *J. Atmos. Sci,* **41,** 1336–1355.

Zege, E. P., A. P. Ivanov, and I. L. Katsev, 1991: *Image Transfer through a Scattering Medium.* Springer-Verlag, 349 pp.

Zender, C. S., B. Bush, S. K. Pope, A. Bucholtz, W. D. Collins, J. T. Kiehl, F. P. J. Valero, and J. Vitko, 1997: Atmospheric absorption during the Atmospheric Radiation Measurement (ARM) Enhanced Shortwave Experiment (ARESE). *J. Geophys. Res.,* **102,** 29 901–29 915.

Zhang, Y., N. Shabanov, Y. Knyazikhin, R. B. Myneni, 2002: Assessing the information content of multiangle satellite data for mapping biomes. II. Theory. *Remote Sens. Environ.,* **80,** 435–446.